Pathways for nonsequential and sequential fragmentation of CO_2^{3+} investigated by electron collision

Enliang Wang,[1,2] Xu Shan,[1,2] Zhenjie Shen,[1,2] Maomao Gong,[1,2] Yaguo Tang,[1,2] Yi Pan,[3]
Kai-Chung Lau,[3] and Xiangjun Chen[1,2,*]

[1]*Hefei National Laboratory for Physical Sciences at Microscale and Department of Modern Physics, University of Science and Technology of China, Hefei, Anhui 230026, China*

[2]*Synergetic Innovation Center of Quantum Information and Quantum Physics, University of Science and Technology of China, Hefei, Anhui 230026, China*

[3]*Department of Biology and Chemistry, City University of Hong Kong, Tat Chee Avenue, Kowloon Tong, Hong Kong, China*

(Received 24 November 2014; published 28 May 2015)

We report nonsequential and sequential fragmentation dynamics of CO_2^{3+} investigated by electron collision at an impact energy of 500 eV. The dissociation mechanisms are clearly distinguished by combined use of the Dalitz plot together with momentum correlation spectra. The angular distributions and kinetic-energy releases (KERs) of different fragmentation processes are obtained. The dissociation channels of higher excited states of the CO_2^{3+} molecular ion are opened, which are quite different from the previous studies of heavy-ion collision [N. Neumann, D. Hant, L. Ph. H. Schmidt, J. Titze, T. Jahnke, A. Czasch, M. S. Schöffler, K. Kreidi, O. Jagutzki, H. Schmidt-Böcking, and R. Dörner, Phys. Rev. Lett. **104**, 103201 (2010)] and intense laser field [C. Wu, C. Wu, D. Song, H. Su, Y. Yang, Z. Wu, X. Liu, H. Liu, M. Li, Y. Deng, Y. Liu, L.-Y. Peng, H. Jiang, and Q. Gong, Phys. Rev. Lett. **110**, 103601 (2013)]. By analyzing KERs together with the help of potential-energy curves exploration at the multireference configuration interaction level, we conclude that the sequential fragmentation occurs in the $^2\Pi$, $^4\Pi$, and $^2\Sigma^+$ states of the CO_2^{3+} ion. The bond length and bond angle are also determined based on the linear fragmentation, indicating that electron impact fragmentation is a potential method to precisely reconstruct the geometry of neutral molecules.

DOI: 10.1103/PhysRevA.91.052711 PACS number(s): 34.80.Gs, 34.50.Gb

I. INTRODUCTION

The investigation of the fragmentation dynamics of molecules is one of the fundamental tasks in physics and chemistry as well as biology. The major challenges in this field are to understand the molecular bond breakage selectivity and to clarify which parameters control bond fission. During the past decade, with the help of rapidly developing imaging techniques [1,2], it was possible to reveal fragmentation dynamics for simple molecules [3], polyatomic molecules [4–6], or even Van-der-Waals clusters [7–9]. In related studies, an interesting and open question is under what conditions the chemical bonds of highly charged polyatomic molecules break through nonsequential or sequential processes. For nonsequential fragmentation, the chemical bonds break simultaneously, which is usually referred to as Coulomb explosion. On the other hand, the molecule dissociates through sequential fragmentation by breaking one bond after another.

Recently, the three-body fragmentation mechanism for $CO_2^{3+} \rightarrow C^+ + O^+ + O^+$ has captured continuous interest in studies of dissociative ionizations by collisions of swift [10,11] and slow heavy ions [12], x rays [13], as well as intense laser fields [14]. Among these studies, only Neumann *et al.* [12] and Wu *et al.* [14] clearly resolved the nonsequential and sequential fragmentation processes of CO_2^{3+} by analyzing momentum correlations among the three fragments. It was found that the amount of energy deposited into the molecular ion plays a key role in switching between the different fragmentation pathways [12]. However, the mechanism to control the pathways still remains unclear due to the complexity of the collision dynamics. An electron impact experiment can also be used to form high charge states of molecules by energy loss of scattered electrons. In the electron scattering process, the incident electron transfers part of its momentum to the target, so basically there is no selection rule for ionization transitions and any final multiple ionization states can be formed in principle. On the other hand, the collision time scale is about 10^{-17}-10^{-16} s for a keV impinging electron, much faster than the nuclear movement time scale, ensuring vertical ionization transition. Coulomb explosion of highly charged molecules is widely used to image molecular geometry [4,15]. The vertical transition of electron impact ionization makes it a potential method to precisely reconstruct the geometry of neutral molecules. Both of these features will shed new light on the investigation of structure and fragmentation dynamics of highly charged molecules. However, the investigation of many-body fragmentation dynamics of the multiple ionized molecule by electron collision is very difficult. For example, the three-body fragmentation process of CO_2^{3+} has been investigated by impact of 12-keV electrons but no evidence was found for sequential fragmentation due to very poor data statistics [16]. This is because the cross section for electron impact triple ionization is extremely low ($\sim 10^{-19}$ cm^2 [17,18]) as compared to the cross section of triple electron capture by collision with highly charged ions ($\sim 10^{-16}$ cm^2 [19]).

In this work, the fragmentation processes of CO_2^{3+} based on electron collision at an impact energy of 500 eV have been investigated. A high-efficiency multicoincidence technique has been developed to largely improve the coincident count rate. This makes the separated detections of sequential and nonsequential fragmentation processes of CO_2^{3+} by electron collision possible for the first time. By careful analysis employing the Dalitz plot [12] and momentum correlation

*xjun@ustc.edu.cn

spectra, as well as precise state-of-the-art *ab initio* potential-energy curves, we are able to clarify the pathways of the fragmentation processes of CO_2^{3+}: the sequential fragmentation mainly takes place through the ground state and the first two low-lying electronic excited states.

II. EXPERIMENTS

All experimental works are carried out using an electron impact ion imaging spectrometer which was built recently in our laboratory. The experimental setup has been described in detail elsewhere [18,20]. Briefly, a pulsed electron beam from a thermal cathode electron gun is injected into the reaction chamber to collide with the gas target effusing from a capillary at the reaction center. The inner and the outer diameters and the length of the capillary are 0.1, 0.3, and 50 mm, respectively. The very high ratio of the length to inner diameter of the capillary enables a well-collimated gas beam. After the collision, a pulsed extraction field (50 V/cm) is applied to extract the ions. A Wiley-Mclaren type time-of-flight (TOF) mass spectrometer [21] is employed to extract the ions with 4π solid angle collection. The lengths of the acceleration and the field-free drift region are 50 and 100 mm, respectively. At the end of the TOF system, a multihit time- and position-sensitive detector (RoentDek DLD 120) [22] is used to detect TOF and impact positions of the ions. A newly developed high-efficiency multicoincidence technique is used to measure the three charged fragments in coincidence. In the experiment, the pulse width and repetition frequency of the electron beam are 10 ns and 15 kHz, respectively. The equivalent beam current is about 15 pA. The background vacuum is better than 5.0×10^{-6} Pa and the working pressure is about 1.0×10^{-4} Pa. The triple coincidence count rate is about 20 Hz, which is far less than the electron-beam repetition frequency, ensuring a high signal to background ratio. In the data analyzing process, the three-body dissociative events are first selected by the correlation analysis of TOFs of ions [20] and are further selected using the δ_p versus kinetic-energy release (KER) (δ_p represents the absolute value of the sum of the momenta of the three final ions) spectrum method [23], which ensures that the three ions originate from same molecule. The three-dimensional momentum vectors of the fragments are reconstructed by their TOFs and detection positions.

III. THEORETICAL CALCULATIONS

We perform state-of-the-art *ab initio* calculations for the potential-energy curves of CO_2^{3+}, including the $^2\Pi$, $^4\Pi$, $^6\Pi$, and $^8\Pi$ and $^2\Sigma^+$, $^4\Sigma^+$, $^6\Sigma^+$, and $^8\Sigma^+$ electronic states, at the MRCI+Q/aug-cc-pVTZ level incorporating the spin-orbital coupling effects. The complete active-space self-consistent field (CASSCF) [24,25] and the internally contracted multireference configuration interaction (MRCI) approaches [26,27] using the aug-cc-pVTZ basis sets [28,29] are performed in the MOLPRO 2010.1 program suite [30]. The $O^+-C^+-O^+$ molecule is kept linear and the two C–O bond lengths are equally stretched during all calculations. The molecular orbitals of linear $O^+-C^+-O^+$ consist of three core orbitals [$2A_g + 1B_{1u}$, corresponding to C($1s$) and O($1s$) orbitals] and 12 valence orbitals [$3A_g + 2B_{3u} + 2B_{2u} + 3B_{1u} + 1B_{2g} + 1B_{3g}$, corresponding to C($2s$), C($2p$), O($2s$), and O($2p$) orbitals]. In the CASSCF calculation, all the core orbitals are kept closed and all the valence orbitals are kept as active orbitals. For the subsequent MRCI calculations, all three core orbitals are kept frozen. The CASSCF and MRCI calculations correlate one Σ^+ state and two Π states in each spin state. All the electronic states are averaged with equal weights in the CASSCF calculations.

IV. RESULTS AND DISCUSSION

In order to analyze the momentum correlation among the three fragments, we employ the Dalitz plot [31]. In the two-dimensional spectrum, the difference between the normalized kinetic energies of the two O^+ ions is plotted in the x axis while the normalized kinetic energy of C^+ is plotted in the y axis:

$$x = \frac{\epsilon_{O_1^+} - \epsilon_{O_2^+}}{\sqrt{3}\epsilon_k}, \tag{1}$$

$$y = \frac{\epsilon_{C^+}}{\epsilon_k} - \frac{1}{3}, \tag{2}$$

where $\epsilon_{O_i^+}$ (i=1, 2); ϵ_{C^+} and ϵ_k are the kinetic energies of O_1^+, O_2^+, and C^+ and the total kinetic energy of the three fragments, respectively. As shown in Fig. 1(a), each point of geometry (x, y) corresponds to a specific momentum correlation among

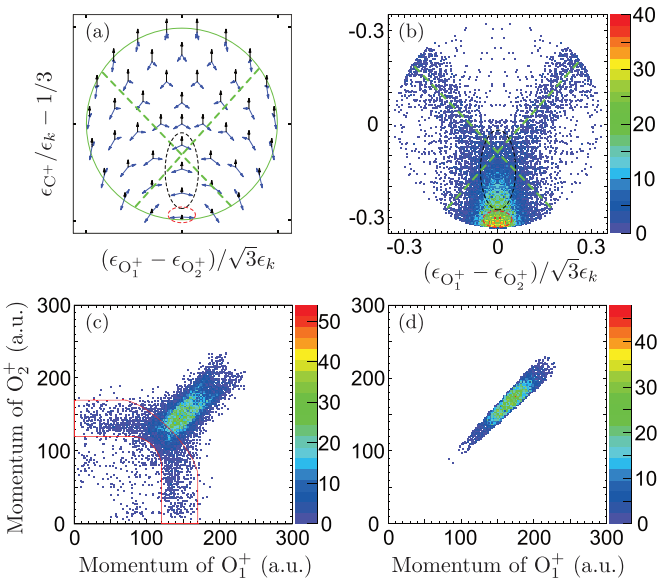

FIG. 1. (Color) (a) Momentum correlation features for various points in the Dalitz plot. (b) Experimental Dalitz plot. The dissociation characteristics of the events labeled by different curves in (b) correspond to the features in (a) marked as the same curves. Red dashed oval: linear dissociation. Black dashed oval: molecular bending dissociation. Green "X" curve: sequential fragmentation. (c) Momentum correlation spectrum of two O^+ ions of the events labeled by the black dashed oval and green "X" curve in (b). The events locate in the red polygon originate from sequential fragmentation. (d) Momentum correlation spectrum of two O^+ ions of the events originating from linear dissociation.

the three fragments. Figure 1(b) shows the experimental Dalitz plot. The main features of the present results are similar to the slow ion collision experiment [12]. The dissociation features of the events marked by the dashed curves in Fig. 1(b) can be obtained with the help of Fig. 1(a). Obviously, the events located in the most intense area (in the red dashed oval) originate from direct linear bond cleavages. The events located on the y axis (marked by a black oval) originate from molecular bending dissociation. The events marked by the "X" curve originate from sequential fragmentation. However, there is serious overlap between the sequential fragmentation and the molecular bending dissociation. Fortunately, the overlap can further be separated by analyzing the momentum correlation between two O^+ ions. For the bending dissociation, as shown in Fig. 1(a), the magnitudes of the momentum vectors of two O^+ ions are equal to each other. While in the case of the sequential fragmentation the two C–O bonds break stepwise and there is no strong correlation between the momentum vectors of two O^+ ions. The momentum correlation spectrum of two O^+ ions from the events marked by the green dashed "X" curve together with the black dashed oval in Fig. 1(b) are shown in Fig. 1(c). The correlation spectrum is composed of two parts. The intense island along the $x = y$ line originates from the molecular bending dissociation. The antennalike structure, which is almost parallel to the x or y axis and is blurred near the $x = y$ line, corresponds to the sequential fragmentation. The events in the red polygon of Fig. 1(c) are chosen as sequential fragmentation events. The momentum correlation spectrum between two O^+ ions originating from the linear dissociation (events in the red dashed oval in the Dalitz plot) is plotted in Fig. 1(d), which also exhibits an island along $x = y$, indicating strong correlation between two O^+ ions.

The total Newton diagram for this three-body fragmentation of $CO_2{}^{3+}$ is shown in Fig. 2(a). The momentum vector of one of the O^+ fragments is fixed along the x axis while the momenta of the second O^+ and C^+ ions are located in the lower and upper halves of the plot. All the momentum vectors of the fragments are normalized to the magnitude of the momentum vector of the first O^+. The two intense islands correspond to the linear or molecular bending dissociation of $CO_2{}^{3+}$. Each of the islands drags a half-circle tail, as marked by a red dashed circle in Fig. 2(a). The circular structure is a direct evidence of the sequential fragmentation. The Newton diagrams for the linear, molecular bending, and sequential fragmentation processes, after being separated by combined analysis employing Dalitz and momentum correlation plots, are shown in Figs. 2(b)–2(d), respectively. Figure 2(b) clearly shows a back-to-back dissociation of O^+ ions, leaving the C^+ ion almost at rest. Figure 2(c) shows the events of molecular bending dissociation. Two O^+ ions dissociate with equal magnitude of momenta. The geometrical rearrangement of the $CO_2{}^{3+}$ ion results in a momentum gain of the C^+ fragment, which leads to the apparent bend angle of the main spots. For the sequential fragmentation, a clear circular structure has been obtained as shown in Fig. 2(d). Figure 3(a) shows the distributions of the correlation angle between the momentum vectors of the two O^+ ions. The total distribution as indicated by the open squares in Fig. 3(a) has a peak value at 164° with a long tail extending to about 60°. A similar

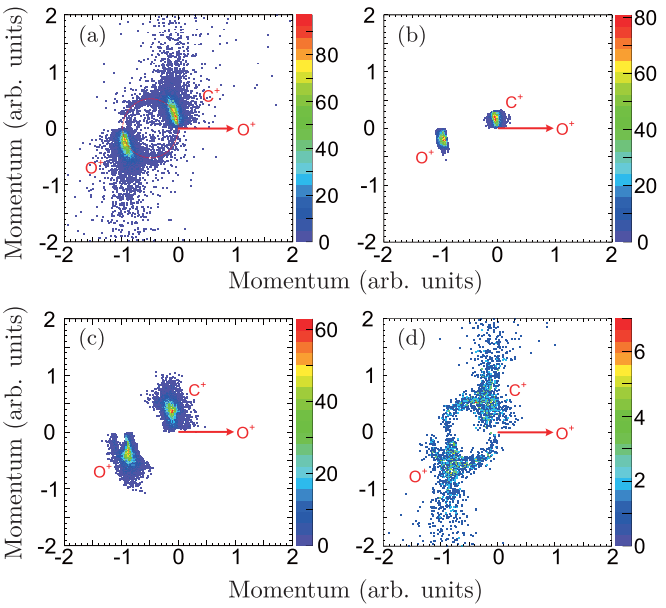

FIG. 2. (Color online) Newton diagrams for (a) all events of three-body fragmentation of $CO_2{}^{3+}$, (b) linear fragmentation, (c) molecular bending dissociation, and (d) sequential fragmentation.

distribution has been observed in the work of Jana *et al.* [11]. However, the physical reason for such distribution was not clear at that time. In this work, the angular distributions for different fragmentation processes have been obtained. All of the linear, molecular bending, and sequential fragmentations exhibit Gaussian type distributions with peak positions at 168.9, 155.5, and 135.5°, respectively, as shown by open stars, open triangles, and solid circles in Fig. 3(a). The linear fragmentation has a sharp distribution with a full width at half maximum of about 12°. Its peak position agrees well with the most probable value of the O–C–O bond angle (172.5°) for the neutral CO_2 molecule [32], which indicates that the two C–O bonds break immediately after ionization without vibrational coupling in the linear fragmentation process. The angular ranges for molecular bending and sequential fragmentations are much wider, which are from 120 to 180° and from 60 to

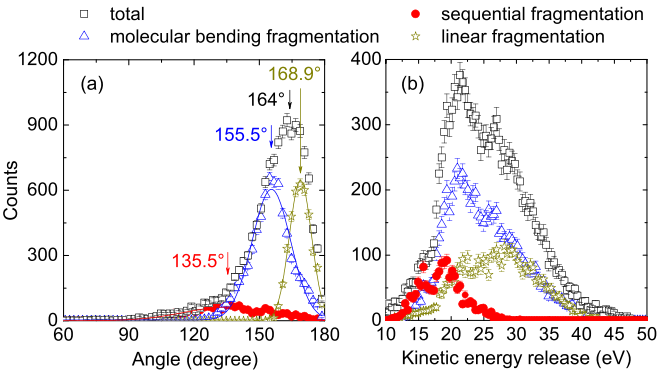

FIG. 3. (Color online) (a) Angular distributions of correlation angle between momentum vectors of two O^+ ions for total events and for events of different fragmentation processes. (b) KER distributions for total events and for different fragmentation processes.

180°, respectively. The sequential fragmentation contributes mainly to the long tail of the total distribution and about 12.6% to all of the three-body dissociative events.

Figure 3(b) shows the KER distributions. The total KER distribution ranges from less than 10 to 50 eV with two peaks at about 21 and 27 eV, and some structures at 10–20 eV. The KER distributions for the linear, molecular bending, and sequential fragmentation processes are also plotted in Fig. 3(b). Generally, the sequential fragmentation tends to release less energy than linear and molecular bending fragmentations; the above result is similar to the results by Neumann *et al.* [12] and Wu *et al.* [14]. Some new features arise in the electron impact three-body dissociations. First, there are significant populations in the high-energy region above 35 eV in the total KER distribution, which is quite different from the previous studies of heavy-ion collision [12] and intense laser fields [14], indicating that more dissociation channels of the excited states for the CO_2^{3+} molecular ion are opened up. Second, both KER distributions for linear and molecular bending fragmentation processes show a peak at ∼21 eV and two structures at ∼27 and ∼29 eV. Third, for the sequential fragmentation, two obvious peaks at 15.8 and 19.0 eV are observed. Interesting, only one broad peak at 17.2 eV for the sequential fragmentation and a broad peak at 20.7 eV for nonsequential fragmentation have been observed by intense laser field [14]. For the slow ion collision experiment [12], on the other hand, a peak at ∼21 eV with a shoulder at ∼19 eV for the sequential dissociation and a broad slope at around 28 eV for nonsequential fragmentation have been observed. In their work, the fragmentation pathways have been identified only through the Dalitz plot. Thus, the events of sequential dissociation were, to some extent, sneaked with some events of molecular bending fragmentation. Our results clearly show that the peak at ∼21 eV can only be ascribed to the nonsequential dissociations.

The theoretical potential-energy curves of CO_2^{3+} are shown in Fig. 4. The $^2\Pi$, $^4\Pi$, and $^2\Sigma^+$ states exhibit a stable potential well at 1.34, 1.40, and 1.30 Å, respectively. As a result, these electronically excited states of CO_2^{3+} are not expected to be broken up by simultaneous stretching of two C–O bonds

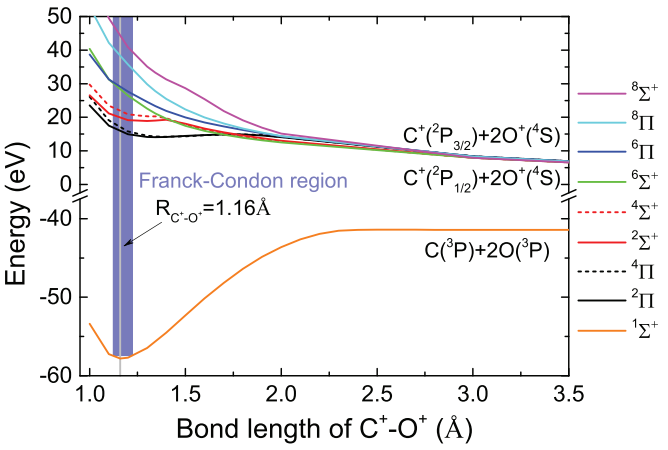

FIG. 4. (Color) Potential-energy curves for the Π and Σ^+ states of CO_2^{3+} at the MRCI + *Q*/aug-cc-pVTZ level with spin-orbit coupling. The potential-energy curve for the ground state ($^1\Sigma^+$) of neutral CO_2 is plotted in the orange curve.

and they are subjected to asymmetric stretching, which leads to the sequential fragmentation. The triple ionizations by electron impact can be regarded as vertical Franck-Condon transitions due to the fast collision time (∼10^{-17}–10^{-16} s). The equilibrium C–O bond length (1.16 Å) of the neutral CO_2 molecule is marked by the vertical gray solid line. Thus the KERs for the dissociations via these three states can be estimated to be ∼16.5 eV ($^2\Pi$ and $^4\Pi$) and ∼19.9 eV ($^2\Sigma^+$), in perfect agreement with the peaks in the observed KER distribution for sequential fragmentation. It is interesting to note that almost no event was observed at around 16 eV in the heavy-ion collision experiment [12], indicating that the multiple electron capture reaction does not form CO_2^{3+} in its lowest two states of $^2\Pi$ and $^4\Pi$. The KER for the dissociation via the $^4\Sigma^+$ state can also be estimated to be ∼21.8 eV, in line with the observed peak at ∼21 eV for the nonsequential dissociations. In the electron impact process, higher excited states of CO_2^{3+} can also be formed, leading to the nonsequential dissociations, and the direct bond breaking process gradually dominates. It is obvious that the dissociations through $^6\Sigma^+$ and $^6\Pi$ states can contribute to the observed structures at 27 and 29 eV in the KER distribution, and the dissociations through higher states of $^8\Sigma^+$ and $^8\Pi$ contribute mainly to the KER distribution in the energy range above 35 eV. The present experimental data also show some small amount of linear fragmentation even for KER less than 20 eV. This is reasonable. The potential curves for the three lowest states of CO_2^{3+} show a low and broad barrier and the energy of the vertical transition point is higher than the height of the barrier. Therefore, there is some probability for these three states to dissociate through linear fragmentation, whose KERs are also around 15.8 and 19.0 eV.

Coulomb explosion of highly charged molecules can be used to image molecular geometry [4,15]. Assuming the linear fragmentation originates from the Coulomb potential, the bond length can be derived to be 1.2 Å for CO_2^{3+} before fragmentation based on the most probable KER of 29 eV, which is quite close to the bond length of 1.16 Å for the neutral CO_2 molecule. Both bond length and bond angle determined in this work agree with the geometry of neutral CO_2 better than the results of the intense laser experiment [14]. This may be due to the structural deformation for CO_2 in intense laser fields [33,34].

V. CONCLUSION

In summary, the fragmentation dynamics of CO_2^{3+} has been studied at an electron impact energy of 500 eV. By combined analysis using the Dalitz plot and momentum correlation spectra, the sequential and nonsequential fragmentation processes have been clearly separated for the first time in the case of electron collision. The KER distributions have been obtained for different fragmentation processes. With the help of potential-energy curves for the ground state and several excited states of CO_2^{3+}, we are able to show that the sequential fragmentation mainly takes place in the ground state ($^2\Pi$) and the first two low-lying electronic excited states ($^4\Pi$ and $^2\Sigma^+$) of the CO_2^{3+} ion. Our study also indicates that, with the improved coincidence technique, electron impact dissociation experiments provide an alternate way to investigate the bond

breaking mechanism for multiple ionized molecules; the unique advantage includes the fact that the accessibility to the final electronic states of the molecular ion by ionization transition is almost unlimited. On the other hand, the convinced vertical transition of the electron impact ionization process and clear separation of direct breakup of the molecule make it a potential method to precisely reconstruct the geometry of neutral molecules.

ACKNOWLEDGMENTS

This work was jointly supported by the National Natural Science Foundation of China (Grants No. 11327404, No. 10734040, No. 11404317, and No. U1432118), the National Basic Research Program of China (Grant No. 2010CB923301), the Fundamental Research Funds for the Central Universities, and China Postdoctoral Science Foundation (Grant No. 2014M561824).

[1] R. Dörner, V. Mergel, O. Jagutzki, L. Spielberger, J. Ullrich, R. Moshammer, and H. Schmidt-Böcking, Phys. Rep. **330**, 95 (2000).

[2] J. Ullrich, R. Moshammer, A. Dorn, R. Dörner, L. Ph. H. Schmidt, and H. Schmidt-Böcking, Rep. Prog. Phys. **66**, 1463 (2003).

[3] T. P. Rakitzis, A. J. van den Brom, and M. H. M. Janssen, Science **303**, 1852 (2004).

[4] M. Pitzer, M. Kunitski, A. S. Johnson, T. Jahnke, H. Sann, F. Sturm, L. Ph. H. Schmidt, H. Schmidt-Böcking, R. Dörner, J. Stohner, J. Kiedrowski, M. Reggelin, S. Marquardt, A. Schießer, R. Berger, and M. S. Schöffler, Science **341**, 1096 (2013).

[5] X. Xie, S. Roither, M. Schöffler, E. Lötstedt, D. Kartashov, L. Zhang, G. G. Paulus, A. Iwasaki, A. Baltuška, K. Yamanouchi, and M. Kitzler, Phys. Rev. X **4**, 021005 (2014).

[6] X. Gong, Q. Song, Q. Ji, H. Pan, J. Ding, J. Wu, and H. Zeng, Phys. Rev. Lett. **112**, 243001 (2014).

[7] T. Jahnke, H. Sann, T. Havermeier, K. Kreidi, C. Stuck, M. Meckel, M. Schöffler, N. Neumann, R. Wallauer, S. Voss, A. Czasch, O. Jagutzki, A. Malakzadeh, F. Afaneh, T. Weber, H. Schmidt-Böcking, and R. Dörner, Nat. Phys. **6**, 139 (2010).

[8] K. Schnorr, A. Senftleben, M. Kurka, A. Rudenko, L. Foucar, G. Schmid, A. Broska, T. Pfeifer, K. Meyer, D. Anielski, R. Boll, D. Rolles, M. Kübel, M. F. Kling, Y. H. Jiang, S. Mondal, T. Tachibana, K. Ueda, T. Marchenko, M. Simon, G. Brenner, R. Treusch, S. Scheit, V. Averbukh, J. Ullrich, C. D. Schröter, and R. Moshammer, Phys. Rev. Lett. **111**, 093402 (2013).

[9] C. Wu, C. Wu, D. Song, H. Su, X. Xie, M. Li, Y. Deng, Y. Liu, and Q. Gong, J. Chem. Phys. **140**, 141101 (2014).

[10] L. Adoui, T. Muranaka, M. Tarisien, S. Legendre, G. Laurent, A. Cassimi, J.-Y. Chesnel, X. Fléhard, F. Frémont, B. Gervais, E. Giglio, and D. Hennecart, Nucl. Instrum. Meth. B **245**, 94 (2006).

[11] M. R. Jana, P. N. Ghosh, B. Bapat, R. K. Kushawaha, K. Saha, I. A. Prajapati, and C. P. Safvan, Phys. Rev. A **84**, 062715 (2011).

[12] N. Neumann, D. Hant, L. Ph. H. Schmidt, J. Titze, T. Jahnke, A. Czasch, M. S. Schöffler, K. Kreidi, O. Jagutzki, H. Schmidt-Böcking, and R. Dörner, Phys. Rev. Lett. **104**, 103201 (2010).

[13] R. K. Singh, G. S. Lodha, V. Sharma, I. A. Prajapati, K. P. Subramanian, and B. Bapat, Phys. Rev. A **74**, 022708 (2006).

[14] C. Wu, C. Wu, D. Song, H. Su, Y. Yang, Z. Wu, X. Liu, H. Liu, M. Li, Y. Deng, Y. Liu, L.-Y. Peng, H. Jiang, and Q. Gong, Phys. Rev. Lett. **110**, 103601 (2013).

[15] Z. Vager, R. Naaman, and E. P. Kanter, Science **244**, 426 (1989).

[16] P. Bhatt, R. Singh, N. Yadav, and R. Shanker, Phys. Rev. A **85**, 042707 (2012).

[17] C. Tian and C. R. Vidal, Phys. Rev. A **58**, 3783 (1998).

[18] E. L. Wang, Z. J. Shen, H. J. Yang, Y. G. Tang, X. Shan, and X. J. Chen, Chin. Phys. B **23**, 113404 (2014).

[19] A. Itoh, N. Imanishi, F. Fukuzawa, N. Hamamoto, S.-I. Hanawa, T. Tanaka, T. Ohdaira, M. Saito, Y. Haruyama, and T. Shirai, J. Phys. Soc. Jpn. **64**, 3255 (1995).

[20] E. L. Wang, X. Shan, Y. F. Shi, Y. G. Tang, and X. J. Chen, Rev. Sci. Instrum. **84**, 123110 (2013).

[21] W. C. Wiley and I. H. McLaren, Rev. Sci. Instrum. **26**, 1150 (1955).

[22] O. Jagutzki, V. Mergel, K. Ullmann-Pfleger, L. Spielberger, U. Spillmann, R. Dörner, and H. Schmidt-Böcking, Nucl. Instrum. Meth. A **477**, 244 (2002).

[23] A. Matsuda, E. J. Takahashi, and A. Hishikawa, J. Chem. Phys. **127**, 114318 (2007).

[24] P. J. Knowles and H.-J. Werner, Chem. Phys. Lett. **115**, 259 (1985).

[25] H.-J. Werner and P. J. Knowles, J. Chem. Phys. **82**, 5053 (1985).

[26] H.-J. Werner and P. J. Knowles, J. Chem. Phys. **89**, 5803 (1988).

[27] P. J. Knowles and H.-J. Werner, Chem. Phys. Lett. **145**, 514 (1988).

[28] T. H. Dunning, J. Chem. Phys. **90**, 1007 (1989).

[29] R. A. Kendall, T. H. Dunning, and R. J. Harrison, J. Chem. Phys. **96**, 6796 (1992).

[30] See H.-J. Werner, P. J. Knowles, G. Knizia, F. R. Manby, M. Schütz, P. Celani, T. Korona, R. Lindh, A. Mitrushenkov, G. Rauhut, K. R. Shamasundar, T. B. Adler, R. D. Amos, A. Bernhardsson, A. Berning, D. L. Cooper, M. J. O. Deegan, A. J. Dobbyn, F. Eckert, E. Goll, C. Hampel, A. Hesselmann, G. Hetzer, T. Hrenar, G. Jansen, C. Köppl, Y. Liu, A. W. Lloyd, R. A. Mata, A. J. May, S. J. McNicholas, W. Meyer, M. E. Mura, A. Nicklaß, D. P. O'Neill, P. Palmieri, D. Peng, K. Pflüger, R. Pitzer, M. Reiher, T. Shiozaki, H. Stoll, A. J. Stone, R. Tarroni, T. Thorsteinsson, and M. Wang, MOLPRO is a package of *ab initio* programs; see http://www.molpro.net.

[31] R. H. Dalitz, Philos. Mag. **44**, 1068 (1953).

[32] B. Siegmann, U. Werner, H. O. Lutz, and R. Mann, J. Phys. B **35**, 3755 (2002).

[33] A. Hishikawa, A. Iwamae, and K. Yamanouchi, Phys. Rev. Lett. **83**, 1127 (1999).

[34] Y. Sato, H. Kono, S. Koseki, and Y. Fujimura, J. Am. Chem. Soc. **125**, 8019 (2003).